

# Failure Analysis of Graphene Sheets with Multiple Stone-Thrower-Wales Defects Using Molecular-Mechanics Based Nonlinear Finite Element Models

Cengiz Baykasoglu<sup>1</sup> , Ata Mugan<sup>2</sup> 

<sup>1</sup>Hitit University, Department of Mechanical Engineering, Corum, TURKEY

<sup>2</sup>Istanbul Technical University, Department of Mechanical Engineering, Istanbul, TURKEY

## ABSTRACT

Experimental studies show that Stone-Thrower-Wales (STW) defects generally exist in graphene sheets (GSs) and these defects considerably affect the fracture strength of GSs. Thus, prediction of failure modes of GSs with STW defects is useful for design of graphene based nanomaterials. In this paper, effects of multiple STW defects on fracture behavior of GSs are investigated by employing molecular mechanics based nonlinear finite element models. The modified Morse potential is used to define the non-linear characteristic of covalent bonds between carbon atoms and geometric nonlinearity effects are considered in models. Different tilting angles of STW defects are considered in simulations. The analysis results showed that the fracture strength of GSs strongly depends on tilting angle of multiple STW defects and the STW defects cause significant strength loss in GSs. The crack initiation and propagation are also studied and brittle failure characteristics are observed for all samples. The results obtained from this study provide some insights into design of GS based-structures with multiple STW defects.

## Keywords:

Graphene sheet, Stone-Thrower-Wales (5-7-7-5) defects, Fracture, Tilting angle, Molecular mechanic

## Article History:

Received: 2017/04/04

Accepted: 2017/06/09

Online: 2017/12/26

**Correspondence to:** Cengiz Baykasoglu  
Hitit University, Department of Mechanical  
Engineering, Cevre Yolu Avenue, 19030,  
Corum, Turkey  
Tel: +90 (364) 227-45-33  
E-Mail: cengizbaykasoglu@hitit.edu.tr

## INTRODUCTION

Graphene sheet (GS) can be defined as a two-dimensional (2-D) sheet of covalently bonded carbon atoms arranged in a honeycomb lattice structure [1]. GSs have been considered as one of the most promising material for technological applications in many areas [2,3] due to its unique mechanical, thermal, electronic, and other physical properties [4-8]. On the other hand, mass production of ideal GSs is very challenging and many kinds of defects such as vacancy and Stone-Thrower-Wales (STW, 5-7-7-5) may emerge during manufacturing processes or may be induced due to stress [9-14]. At this point, several studies reveal that vacancy and STW defects significantly affect the fracture behavior of GSs [15, 16]. Thus, prediction of fracture characteristic of GSs with different kinds of defects is very crucial for design of graphene based nanomaterials.

Physical or experimental measurements for prediction of fracture behavior of carbon-based nanostructures are very limited due to challenges associated with designing experiments at the nanoscale. Thus,

computational modelling approaches are widely used to investigate fracture behavior of these structures. At this point, atomistic modelling approaches such as Molecular Dynamics (MD) and Molecular Mechanics (MM) methods are commonly used to investigate the mechanical performance of defected GSs and carbon nanotubes (CNTs) [15-25]. Relevant works in literature are summarized as follows. Troya et al. [20] investigated effects of STW defects on failure stress of CNTs by using Quantum Mechanics (QM) method. Chandra et al. [21] examined local elastic properties of CNTs having STW defects. In another study, Mielke et al. [22] predicted the fracture strain and stress of STW-defected CNTs using MD and QM methods. Belytschko et al. [23] studied failure behavior of STW defected CNTs using atomistic simulations. Besides, Wang et al. [24] studied the failure of vacancy and STW defected GSs using MD simulations. Furthermore, He et al. [25] studied the effects of multiple STW defects on the mechanical performance of GSs employing MD simulations. All aforementioned atomistic studies [20-25] showed that the presence of STW defects negatively affect the mechanical perfor-

mance of CNTs and GSs.

On the other hand, in spite of their accuracy, QM and MD approaches are computationally very expensive and not suitable for modeling large scale models. Hence, MM based modeling approaches have been widely used to investigate mechanical properties of defected graphene based structures due to their computational efficiencies [26-34]. These approaches construct a bridge between the MM and continuum mechanics by energy equivalence [35-37]. In a typical MM based model, the covalent bonds between carbon atoms are simulated using different kinds of structural elements such as springs, beams and rods [26-37]. Relevant MM based modeling studies are summarized as follows: Tserpes et al. [26] developed a Finite Element (FE) based failure model to examine the failure behavior of pristine and vacancy-defected CNTs. Tserpes et al. [27] also examined the effects of STW-defects on the fracture performance of CNTs and the reduction in failure strength is predicted in the range of range 18 to 25 %. Xiao et al. [28] used an atomistic based FE approach to predict failure behavior of STW- defected GSs and CNTs and the reduction in failure strength is predicted in the range of 12 to 32 %. Besides, Xiao et al. [29] also examined the tensile behavior of GSs and CNTs having multiple STW defects. Moshrefzadeh-Sani et al. [30] proposed a continuum model for STW-defected CNTs in which an STW defect is replaced by a crack with a definite length. Furthermore, Wang et al. [31] examined the mechanical properties of graphene nanofilms having STW defects using atomistic mechanics based FE models. Moreover, we developed MM based nonlinear FE models and examined failure behavior of GSs and CNTs [32-34].

Although there are some published works about failure behavior of STW-defected GSs and CNTs, only a few studies are initiated to investigate fracture behavior of multiple STW-defected GSs [25, 29]. On the other hand, there is no comparative study on the fracture behavior of multiple STW defected-GSs by the use of MM based nonlinear FE models. Motivated by these facts, the fracture properties of multiple STW defected GSs are investigated using MM based nonlinear FE models in which both geometric and material nonlinearities are considered. Different tilting angles which are the angle between tensile direction and axis of STW defects are considered in simulations. The analysis results reveal that the tilting angle has a significant effect on fracture behavior of GSs and the STW defects considerable affect the failure behavior of GSs. Besides, the fracture initiation and propagation patterns are also examined and diagonal crack propagation patterns are observed for all cases. The brittle fracture characteristics are also observed for STW defected-GSs

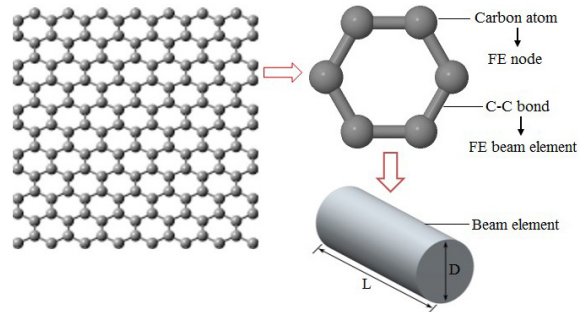


Figure 1. FE modeling of graphene

## COMPUTATIONAL METHODOLOGY

We already developed a MM based nonlinear FE model to investigate failure behavior of carbon based nanostructures (e.g., CNTs and GSs) in our previous works [32-34]. In this study, the similar approach with Refs. [32-34] is employed to examine fracture behavior of multiple STW-defected GSs. Namely, 2-D Euler–Bernoulli (EB) beam elements are used to model bonds between carbon atoms and the characteristic of C-C bonds are simulated by employing the modified Morse interatomic potential (i.e., Fig. 1).

Nonlinear geometric effects are also included in the models. At this point, incremental displacement loading is applied to zigzag direction of GSs (i.e. Fig. 3), stiffness of the EB elements are calculated using the proposed atomistic potential and updated with the atomic positions at each incremental loading step. The stiffness matrix of 2-D EB beam element is given as [38]

$$\mathbf{K} = \begin{bmatrix} \frac{EA}{L} & 0 & 0 & -\frac{EA}{L} & 0 & 0 \\ 0 & \frac{12EI}{L^3} & \frac{6EI}{L^2} & 0 & \frac{12EI}{L^3} & \frac{6EI}{L^2} \\ 0 & \frac{6EI}{L^2} & \frac{4EI}{L} & 0 & \frac{6EI}{L^2} & \frac{2EI}{L} \\ -\frac{EA}{L} & 0 & 0 & \frac{EA}{L} & 0 & 0 \\ 0 & \frac{12EI}{L^3} & \frac{6EI}{L^2} & 0 & \frac{12EI}{L^3} & \frac{6EI}{L^2} \\ 0 & \frac{6EI}{L^2} & \frac{2EI}{L} & 0 & \frac{6EI}{L^2} & \frac{4EI}{L} \end{bmatrix} \quad (1)$$

where  $E$  is the elasticity modulus,  $A$  is the cross-sectional area of beam element,  $I$  is the inertia moment and  $L$  is the initial length of a covalent bond. The initial secant modulus of EB beam elements is taken as 6.93 TPa which is calculated from the stress ( $\sigma$ ) – strain ( $\epsilon$ ) curve of covalent bond using the modified Morse potential [32]. The geometric parameters of beam elements are given in Table 1.

Table 1. Geometric parameters of the EB beam element [39].

Thickness of beam, $D$	1.47 Å
Cross-sectional area of beam, $A$	1.687 Å <sup>2</sup>
Moment of inertia of beam, $I$	0.22682 Å <sup>4</sup>
Initial length of beam, $L$	1.421 Å

**Table 2.** The modified Morse potential parameters [23].

$r_0$	$1.421 \text{ \AA}$	$\partial_0$	$2.094 \text{ rad}$
$\beta$	$2.625 \text{ \AA}^{-2}$	$k\theta$	$0.9 \times 10^{-8} \text{ N\AA/rad}^2$
$D_e$	$6.03105 \times 10^{-9} \text{ N\AA}$	$k_{sextic}$	$0.754 \text{ \AA}^4$

The atomistic interactions are basically governed by the bond stretching and bond angle-bending terms for in-plane deformations problems of GSs. Hence, the modified Morse potential includes bond stretching ( $U_r$ ) and angle-bending ( $U_\theta$ ) energy terms as given by

$$U_{total} = \sum U_r + \sum U_\theta \quad (2)$$

$$U_r = D_e \left\{ \left[ 1 - e^{-\beta(r-r_0)} \right]^2 - 1 \right\} \quad (3)$$

$$U_\theta = \frac{1}{2} k_\theta (\theta - \theta_0)^2 + \left[ 1 + k_{sextic} (\theta - \theta_0)^4 \right] \quad (4)$$

where  $r$  is the current C-C bond length,  $\theta$  is the current angle of adjacent bond,  $\beta$  is the constant which controls the width of potential and  $D_e$  denotes the dissociation energy. The parameters of the modified Morse potential are presented in Table 2. Detailed information on the modified Morse potential and its parameters can be found in [23].

The bond stretching ( $U_r$ ) term has the dominant effect on fracture behavior of GSs. Hence, the angle-bending term (i.e. Eq. 4) is neglected in analyses as done by the following references [26, 27, 32-34, 40]. By differentiating Eq. 3 by respect to bond length ( $r$ ), the stretching force of C-C bonds is defined as follows:

$$F = 2\beta D_e (1 - e^{-\beta(r-r_0)}) e^{-\beta(r-r_0)} \quad (5)$$

Fig. 2 shows the relationship between force and bond strain for the covalent bond between carbon atoms. Belytschko et al. [23] investigated the fracture behavior of CNTs and reported that the fracture depends mainly on the inflection point of interatomic potential. Thus, after the inflection point, the shape of the modified Morse potential function is not critical since material damage takes place. Similarly, in this study, the cut-off distance value of  $1.69 \text{ \AA}$

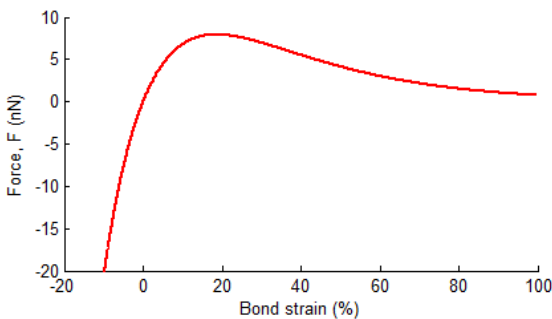


**Figure 2.** Force-strain curve of modified Morse interatomic potential

which corresponds to the inflection point at approximately 19 % strain (i.e. see Fig. 2) is employed in analysis. Beyond this value, the shape of the modified Morse potential is not critical because bond fracture occurs [23].

Geometries of STW-defected GS models are constructed using a Matlab code. Sufficiently large GS models are used in analyses in order to prevent the end effects. Finally, the GSs models having the dimensions of  $125.52 \times 126.46$  is employed in analysis. The models contain 6180 atoms and 9159 covalent bonds. The details about the modeling approach and update procedure can be found in [32, 33]. Fig. 3 shows the proposed STW-defected GS model.

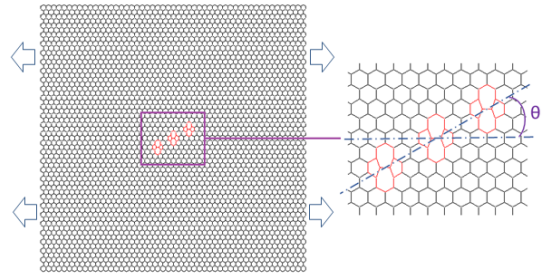


**Figure 3.** The defected GSs having three STW-defects and definition of the tilting angle

## RESULTS AND DISCUSSION

In numerical models, all the atoms (i.e., nodes) at the one end (in this study, armchair edge) of GSs are fixed and the incremental displacement loading is applied to the atoms at the other end. The stiffness and nodal positions (atomic positions) of each element (i.e., bond) are updated at each incremental loading step. Stress-strain curve of the C-C bond are shown in Fig. 4.

When a bond breaks, then its stiffness matrix is multiplied by a very small number to simulate bond breaking phenomena. The total strain and stress are respectively calculated using the following equations:

$$\varepsilon = \frac{(L - L_0)}{L_0}, \quad \sigma = \frac{F}{wt} \quad (6)$$

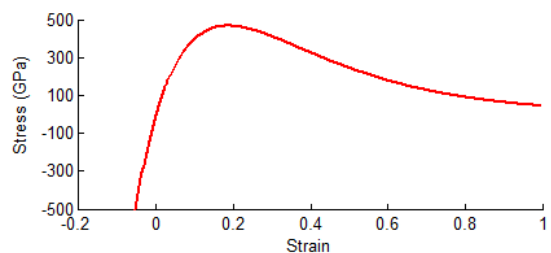


**Figure 4.** Stress-strain curve of C-C bond

where,  $L$  is the current length,  $L_0$  is the initial length,  $w$  is the width,  $t$  is the thickness of the GSs and  $F$  is the applied tensile force which is calculated by summing of the reaction forces at the fixed nodes. The thickness of the GSs is considered as  $3.4 \text{ \AA}$ . In addition, strain increment of  $0.1 \%$  is employed in the analyses. In which, we assume that one STW defect is located in the middle of the GSs and other two STW defects are located around the middle defects. Different tilting angle are considered in analyses and the distance between the STW defects is selected to be constant (i.e. Fig. 3).

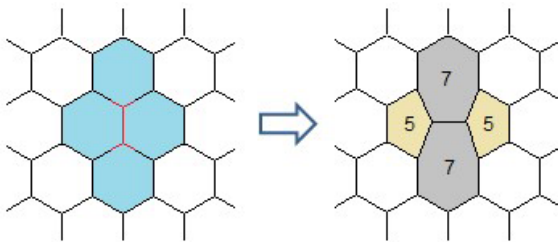


**Figure 5.** Schematic model showing the transformation of four adjacent hexagons into STW defect

The STW (5-7-7-5) is a topological defect [41,42] and may be induced due to stress. Namely, when GSs are subjected to tensile loading, GSs release their excess tension via formation of STW defects. Nardelli et al. [13, 14] pointed out that defect nucleation happens via STW transformation at the strain of  $5\%$  in armchair CNTs and somewhat later in GSs. Besides, Zhang et al. [43] showed that the STW transformation happens at strain of  $6\%$  for armchair CNTs. In this work, we proposed critical strain for the formation of the STW defects as  $6\%$ . At this point, we used the pristine GSs up to critical strain of  $6\%$  and then, the corresponding bond configurations are modified at this formation strain. After STW transformation occurs, four hexagons change into two heptagons and two pentagons. The total number of the atoms does not change in this transformation. Fig. 5 shows schematic representation of STW (5-7-7-5) formation. Also note that, after the STW transformation occurs, a

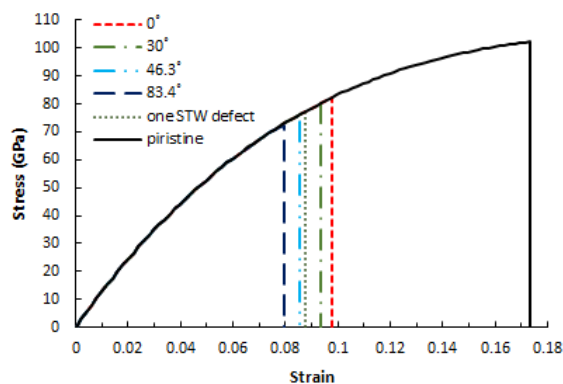


**Figure 6.** Tensile stress–strain curves of GSs having STW-defects

prestrain is employed to minimize energy configuration of atoms and calculation is continued until fracture happens.

Fig. 6 illustrates stress–strain curves of some selected multiple STW-defected GSs for different tilting angles. It can be observed in Fig. 6 that the failure stress and failure strain values of defect-free (pristine) GSs (which are respectively  $102.15 \text{ GPa}$  and  $0.174$ ) reduced by the presence of STW-defects due to the stress concentration in vertical bonds that occurs after bond rearrangement. Hence, more STW defects may cause higher stress concentration at the multiple STW defects areas. The fracture stress of pristine GSs the reduced by  $19.5\text{--}29.2 \%$ , if three STW defects exist in the GS structure. It is also seen in Fig. 6 that the fracture stress of GSs decreases with the increasing tilting angle. Namely, the fracture stress value of multiple STW-defected GSs having the tilting angle of  $0^\circ$  is approximately  $14 \%$  higher than STW-defected GSs having the tilting angle of  $83.4^\circ$ . He et al. [25] predicted that the fracture strength value of two STW-defected GSs having the tilting angle of  $0^\circ$  is approximately  $14.1 \%$  higher than that of  $83.4^\circ$ . Thus, our prediction is in good agreement with the MD simulation result in Ref. [25].

On the other hand, as can be observed in Fig. 6, the stress curve suddenly drops to zero when the stress reaches to a certain value. Thus, it is concluded that the failure of pristine and defected GSs are brittle type which is in good agreement with the results of [23–28].

Fig. 7 shows the fracture stress of STW-defected GSs having different tilting angles. In addition, the fracture stress value of one STW-defected GS (i.e.,  $77.88 \text{ GPa}$ ) is also given in Fig. 7. It is observed that the fracture stresses of multiple STW-defected GSs are higher than that of one STW defected GS when tilting angle is smaller than approximately  $45^\circ$ . It is also observed that the reduction of the fracture stress values in the range  $30^\circ < \theta < 60^\circ$  is higher than other angle ranges. He et al. [25] showed that the ultimate strength of graphene sheets decreases much slower when the angle is larger than  $55.4^\circ$ . Hence, our prediction is in good agreements with the MD result of Ref. [25].

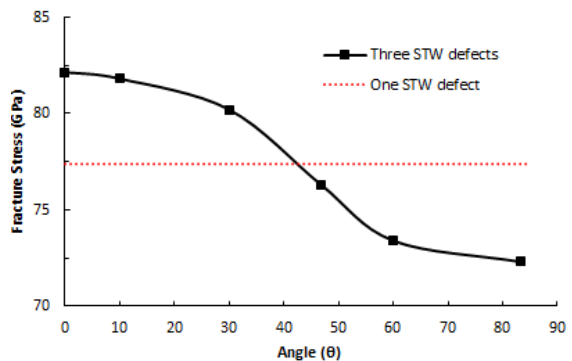


**Figure 7.** Comparison of the fracture stress of multiple STW-defected GSs for different tilting angles with the one STW-defected GS

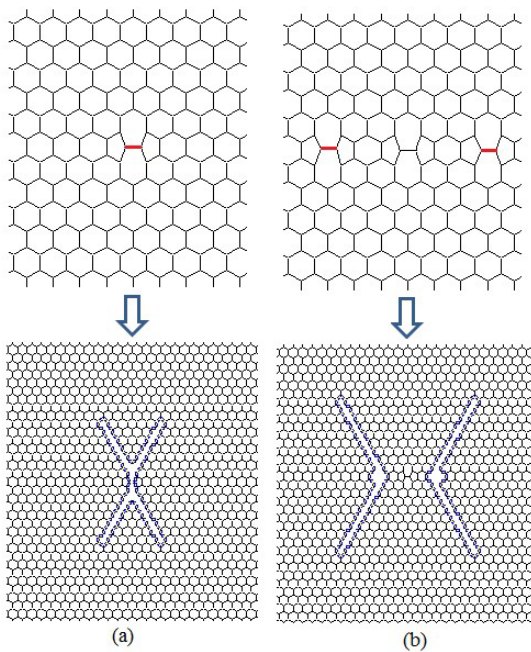


**Figure 8.** Fractured profile of the one (left) and multiple STW-defected GS (tilting angle of  $0^\circ$ ) (right) under tension

The fracture initiation and post failure characteristic of STW-defected GSs can be predicted by employing the proposed approach. Fig. 8 shows the crack initiation and propagation directions (deletion of failed bonds based on the proposed failure criterion) of one and multiple STW-defected GS. As can be seen in Fig. 8a, for the GSs with one STW defect, the first bond fracture is initiated from the longitudinal bond which connects the two pentagons. Then, the fracture propagated in the  $\pm 45^\circ$  maximum shear stress directions. The similar propagation patterns are also observed in Ref. [23, 28] for STW defected graphitic structures. On the other hand, as can be observed in Fig. 8b that the failure initiated from the right and left horizontal bonds of GS having three STW defects (i.e., represented in red color) and continued along the diagonal crack paths similar to the one STW defected sample. This prediction is reasonable since stresses are concentrated at the left and right STW-defected regions and the no bond failure is observed in the region around the middle STW-defect. Once first bond failure initiated, stresses are concentrated on the diagonal neighboring bonds causing subsequent fractures. The similar fracture patterns are also observed for other tilting angles. This failure patterns which shown in Fig. 8 is also in good agreement with the results in Ref. [23,29].

## CONCLUSION

In this paper, the fracture behavior of multiple STW-defected GSs is investigated using MM based nonlinear finite element models. The effect of tilting angle on fracture characteristic of GS is also investigated in the

analyses. The results show that multiple STW defects cause significant reduction in strength values of the GS structures. Namely, the strength of pristine GSs is reduced by 19.5- 29.2 % if three STW defects exist in the structure. It is observed that the tilting angle ( $\theta$ ) is also an important geometric parameter and strongly affects the fracture strength of GSs. Higher reduction in fracture strength is observed in the range  $30^\circ < \theta < 60^\circ$ . Besides, crack initiation and propagation are examined. It is concluded that the failure of GSs are in a brittle manner.

## REFERENCES

1. Meyer, J. C., Geim, A. K., Katsnelson, M. I., Novoselov, K. S., Booth, T. J., & Roth, S. The structure of suspended graphene sheets. *Nature* 446(7131) (2007) 60–63.
2. Huang, X., Yin, Z., Wu, S., Qi, X., He, Q., Zhang, Q., Yang, Q., Boey, F., & Zhang, H. Graphene-based materials: synthesis, characterization, properties, and applications. *Small* 7(14) (2011) 1876–1902.
3. Avouris, P., & Dimitrakopoulos, C. Graphene: synthesis and applications. *Materials today* 15(3) (2012) 86–97.
4. Lee, C., Wei, X., Kysar, J. W., & Hone, J. Measurement of the elastic properties and intrinsic strength of monolayer graphene. *Science* 321(5887) (2008) 385–388.
5. Neto, A. C., Guinea, F., Peres, N. M. R., Novoselov, K. S., & Geim, A. K. The electronic properties of graphene. *Reviews of modern physics* 81(1) (2009) 109.
6. Pop, E., Varshney, V., & Roy, A. K. Thermal properties of graphene: Fundamentals and applications. *MRS bulletin* 37(12) (2012) 1273–1281.
7. Civalek, Ö., & Akgöz, B. Vibration analysis of micro-scaled sector shaped graphene surrounded by an elastic matrix. *Computational Materials Science* 77 (2013) 295–303.
8. Akgöz, B., & Civalek, Ö. Free vibration analysis for single-layered graphene sheets in an elastic matrix via modified couple stress theory. *Materials & Design* 42 (2012) 164–171.
9. Banhart, F., Kotakoski, J., & Krasheninnikov, A. V. Structural defects in graphene. *ACS nano* 5(1) (2010) 26–41.
10. Lee, G. D., Wang, C. Z., Yoon, E., Hwang, N. M., Kim, D. Y., & Ho, K. M. Diffusion, coalescence, and reconstruction of vacancy defects in graphene layers. *Physical review letters* 95(20) (2005) 205501.
11. Lusk, M. T., & Carr, L. D. Creation of graphene allotropes using patterned defects. *Carbon* 47(9) (2009) 2226–2232.
12. Sun, Y. J., Ma, F., Ma, D. Y., Xu, K. W., & Chu, P. K. Stress-induced annihilation of Stone-Wales defects in graphene nanoribbons. *Journal of Physics D: Applied Physics* 45(30) (2012) 305303.
13. Nardelli, M. B., Yakobson, B. I., & Bernholc, J. Mechanism of strain release in carbon nanotubes. *Physical Review B* 57(8) (1998) R4277.
14. Nardelli, M. B., Yakobson, B. I., & Bernholc, J. Brittle and ductile behavior in carbon nanotubes. *Physical review letters* 81(21) (1998) 4656.
15. Zhang, T., Li, X., & Gao, H. Fracture of graphene: a review. *International Journal of Fracture* 1–31 (2015).
16. Xu, L., Wei, N., & Zheng, Y. Mechanical properties of highly defective graphene: from brittle rupture to ductile fracture.

- Nanotechnology 24(50) (2013)505703.
17. Cao, G. Atomistic studies of mechanical properties of graphene. *Polymers* 6(9) (2014) 2404–2432.
  18. Ansari, R., Motevalli, B., Montazeri, A., & Ajori, S. Fracture analysis of monolayer graphene sheets with double vacancy defects via MD simulation. *Solid State Communications* 151(17) (2011) 1141–1146.
  19. Yanovsky, Y. G., Nikitina, E. A., Karnet, Y. N., & Nikitin, S. M. Quantum mechanics study of the mechanism of deformation and fracture of graphene. *Physical Mesomechanics* 12(5) (2009) 254–262.
  20. Troya, D., Mielke, S. L., & Schatz, G. C. Carbon nanotube fracture-differences between quantum mechanical mechanisms and those of empirical potentials. *Chemical Physics Letters* 382(1) (2003) 133–141.
  21. Chandra, N., Namila, S., & Shet, C. Local elastic properties of carbon nanotubes in the presence of Stone–Wales defects. *Physical Review B* 69(9) (2004) 094101.
  22. Mielke, S. L., Troya, D., Zhang, S., Li, J. L., Xiao, S., Car, R., Ruoff, R.S., Schatz, G. C., & Belytschko, T. The role of vacancy defects and holes in the fracture of carbon nanotubes. *Chemical Physics Letters* 390(4) (2004) 413–420.
  23. Belytschko, T., Xiao, S. P., Schatz, G. C., & Ruoff, R. S. Atomistic simulations of nanotube fracture. *Physical Review B* 65(23) (2002) 235430.
  24. Wang, M. C., Yan, C., Ma, L., Hu, N., & Chen, M. W. Effect of defects on fracture strength of graphene sheets. *Computational Materials Science* 54 (2012) 236–239.
  25. He, L., Guo, S., Lei, J., Sha, Z., & Liu, Z. The effect of Stone-Thrower-Wales defects on mechanical properties of graphene sheets-A molecular dynamics study. *Carbon* 75 (2014) 124–132.
  26. Tserpes, K. I., Papanikos, P., & Tsirkas, S. A. A progressive fracture model for carbon nanotubes. *Composites Part B: Engineering* 37(7) (2006) 662–669.
  27. Tserpes, K. I., & Papanikos, P. The effect of Stone–Wales defect on the tensile behavior and fracture of single-walled carbon nanotubes. *Composite Structures* 79(4) (2007) 581–589.
  28. Xiao, J. R., Staniszewski, J., & Gillespie, J. W. Fracture and progressive failure of defective graphene sheets and carbon nanotubes. *Composite structures* 88(4) (2009) 602–609.
  29. Xiao, J. R., Staniszewski, J., & Gillespie, J. W. Tensile behaviors of graphene sheets and carbon nanotubes with multiple Stone–Wales defects. *Materials Science and Engineering: A*, 527(3) (2010) 715–723.
  30. Moshrefzadeh–Sani, H., Saboori, B., & Alizadeh, M. A Continuum Model For Stone–wales Defected Carbon Nanotubes. *International Journal of Engineering–Transactions C: Aspects* 28(3) (2015) 433.
  31. Wang, S. P., Guo, J. G., & Zhou, L. J. Influence of Stone–Wales defects on elastic properties of graphene nanofilms. *Physica E: Low–dimensional Systems and Nanostructures* 48 (2013) 29–35.
  32. Baykasoğlu, C., & Mugaň, A. Nonlinear fracture analysis of single-layer graphene sheets. *Engineering Fracture Mechanics* 96 (2012) 241–250.
  33. Baykasoğlu, C., Kirca, M., & Mugaň, A. Nonlinear failure analysis of carbon nanotubes by using molecular–mechanics based models. *Composites Part B: Engineering* 50 (2013) 150–157.
  34. Baykasoğlu, C., & Mugaň, A. Coupled molecular/continuum mechanical modeling of graphene sheets. *Physica E: Low–dimensional Systems and Nanostructures* 45 (2012) 151–161.
  35. Odegard, G. M., Gates, T. S., Nicholson, L. M., & Wise, K. E. Equivalent–continuum modeling of nano–structured materials. *Composites Science and Technology* 62(14) (2002) 1869–1880.
  36. Li, C., & Chou, T. W. A structural mechanics approach for the analysis of carbon nanotubes. *International Journal of Solids and Structures* 40(10) (2003) 2487–2499.
  37. Baykasoğlu, C., & Mugaň, A. Dynamic analysis of single-layer graphene sheets. *Computational Materials Science* 55 (2012) 228–236.
  38. Liu, G. R., & Quek, S. S. *The finite element method: a practical course*. Butterworth–Heinemann, 2013.
  39. Tserpes K I and Papanikos P. Finite element modeling of single-walled carbon nanotubes *Composites Part B* 36 (2005) 468–477.
  40. Baykasoğlu, C., Icer, E., Celebi, A. T., & Mugaň, A. Nonlinear fracture analysis of carbon nanotubes with stone-wales defects, 3rd South–East European Conference on Computational Mechanics, SEECCM 2013; Kos Island; Greece; 12 June 2013, (2013) 446–454.
  41. Stone, A. J., & Wales, D. J. Theoretical studies of icosahedral C 60 and some related species. *Chemical Physics Letters*, 128(5) (1986) 501–503.
  42. Thrower, P.A. The study of defects in graphite by transmission electron microscopy. *Chemistry and Physics of Carbon* 5 (1969) 217–320.
  43. Zhang, P., Lammert, P. E., & Crespi, V. H. Plastic deformations of carbon nanotubes. *Physical Review Letters*, 81(24) (1998) 5346.